

Intermediate resolution H β spectroscopy and photometric monitoring of 3C 390.3

I. Further evidence of a nuclear accretion disk *

A.I. Shapovalova¹, A.N. Burenkov¹, L. Carrasco^{2,3}, V.H. Chavushyan², V.T. Doroshenko⁴, A.M. Dumont⁵, V.M. Lyuty⁴, J.R. Valdés², V.V. Vlasuyk¹, N.G. Bochkarev⁴, S. Collin⁵, F. Legrand², V.P. Mikhailov¹, O.I. Spiridonova¹, O. Kurtanidze⁶, and M.G. Nikolashvili⁶

¹ Special Astrophysical Observatory of the Russian AS, Nizhnij Arkhyz, Karachaevo-Cherkessia, 369167, Russia
 e-mail: ashap@sao.ru

² Instituto Nacional de Astrofísica, Óptica y Electrónica, Apartado Postal 51, C.P. 72000, Puebla, Pue., México
 e-mail: carrasco@inaoep.mx

³ Observatorio Astronómico Nacional, UNAM, Apartado Postal 877, C.P. 22860, Ensenada B.C., México

⁴ Sternberg Astronomical Institute, University of Moscow, Universitetskij Prospect 13, Moscow 119899, Rusia

⁵ DAEC, Observatoire de Paris, section de Meudon, Place Jansen, F-92195 Meudon, France

⁶ Abastumani Astrophysical Observatory, Georgian AS, Mt. Kanobili, 383762, Abastumani, Georgia

Received: February 21, 2001 / Accepted: June 13, 2001

Abstract. We have monitored the AGN 3C 390.3 between 1995 and 2000. A historical B-Band light curve dating back to 1966, shows a large increase in brightness during 1970 – 1971, followed by a gradual decrease down to a minimum in 1982. During the 1995–2000 lapse the broad H β emission and the continuum flux varied by a factor of ≈ 3 . Two large amplitude outbursts, of different duration, in continuum and H β light were observed i.e.: in October 1994 a brighter flare that lasted ≈ 1000 days and in July 1997 another one that lasted ≈ 700 days were detected. The response time lag of the emission lines relative to flux changes of the continuum, has been found to vary with time i.e. during 1995–1997 a lag of about 100 days is evident, while during 1998–1999 a double valued lag of ≈ 100 days and ≈ 35 days is present in our data. The flux in the H β wings and line core vary simultaneously, a behavior indicative of predominantly circular motions in the BLR. Important changes of the H β emission profiles were detected: at times, we found profiles with prominent asymmetric wings, as those normally seen in Sy1s, while at other times, we observe profiles with weak almost symmetrical wings, similar to those of Sy1.8s. We further dismiss the hypothesis that the double peaked H β profiles in this object originate in a massive binary BH. Instead, we found that the radial velocity difference between the red and blue bumps is anticorrelated with the light curves of H β and continuum radiation. This implies that the zone that contributes with most of the energy to the emitted line, changes in radius within the disk. The velocity difference increases, corresponding to smaller radii, as the continuum flux decreases. When the continuum flux increases the hump velocity difference decreases. These transient phenomena are expected to result from the variable accretion rate close to the central source. The optical continuum and the H β flux variations might be related to changes in X-ray emission modulated by a variable accretion rate, changing the surface temperature of the disk, as a result of a variable X-ray irradiation (Ulrich, 2000). Theoretical H β profiles were computed for an accretion disk, the observed profiles are best reproduced by an inclined disk (25°) whose region of maximum emission is located roughly at $200 R_g$. The mass of the black hole in 3C 390.3, estimated from the reverberation analysis is $M_{rev} \approx 2.1 \times 10^9 M_\odot$, 5 times larger than previous estimates (Wandel et al.1999).

Key words. galaxies: active – galaxies: Seyfert – galaxies: individual (3C 390.3) – line: profiles

1. Introduction

Quasars and Active Galactic Nuclei (AGNs) are amongst the most luminous objects in the Universe and provide a unique test case for several processes of astrophysical importance. A relevant characteristic of some of these ob-

Send offprint requests to: A.I. Shapovalova or L. Carrasco

* based on observations carried out at SAO RAS, Guillermo Haro, Abastumani and Sternberg Observatories.

jects is a variable broad emission line spectrum. The region where broad lines are formed (hereinafter BLR) is rather close to the central engine and may hold basic information to the understanding of the formation and fueling of AGNs and quasars, a process not yet fully understood.

Long temporal baseline spectral monitoring of the nuclei of some AGNs has revealed a time lag in the response of the broad emission lines relative to flux changes of the continuum. This lag depends on the size, geometry and physical conditions of the emitting region. Thus, the search for correlations between nuclear continuum changes and flux variations of the broad emission lines may serve as a tool for mapping the geometrical and dynamical structure of the BLR (see Peterson, 1993 and references therein). From the study of the responses of lines of different ions, to changes of the nuclear continuum and the comparison of these data with photoionization model predictions, one could infer some of the physical conditions in the BLR as a function of the distance from the central source (Dumont et al. 1998).

From changes of the broad emission line profiles, we could distinguish, in principle, different kinematical models for the BLRs, including cases in which matter is undergoing accelerated motions, ie. falling or outflowing, keplarian rotation in the gravitational field of the central body, and some others (Bochkarev & Antokhin 1982; Blanford & McKee 1982; Antokhin & Bochkarev 1983).

During the last decade, the study of the BLRs in some objects has met considerable success, mainly due to an increasing number of coordinated multiwavelength monitoring campaigns through the international "AGN Watch" program. This program has provided data with good temporal frequency and coverage for a number of selected Seyfert galaxies: NGC 5548 (Clavel et al. 1991; Peterson et al. 1991, 1993, 1994, 1999; Maoz et al. 1993; Dietrich et al. 1993; Korista et al. 1995; Chiang et al. 2000); NGC 3783 (Reichert et al. 1994; Stirpe et al. 1994; Alloin et al. 1995); NGC 4151 (Crenshaw et al. 1996; Kaspi et al. 1996; Warwick et al. 1996; Edelson et al. 1996); Fairall 9 (Rodriguez-Pascual et al. 1997; Santos-Lleo et al. 1997); NGC7469 (Wanders et al. 1997; Collier et al. 1998) and 3C 390.3 (Leighly et al. 1997; Dietrich et al. 1998; O'Brien et al. 1998). It has been found that a significant part of the BLR variability can be associated with a region located within some light weeks from the central source. The inferred BLR extent is comparable to the size of an hypothetical accretion disk surrounding a supermassive black hole. Therefore, at least part of the flux from the BLR arises, apparently, from the accretion disk itself (Laor & Netzer 1989, Dumont & Collin-Souffrin 1990a, 1990b; Zheng et al. 1991; Hubeny et al. 2000). It is also found that, the higher ionization lines respond faster to continuum flux changes than those of lower ionization and that the optical and ultraviolet continua vary without a significant time lag between them.

The results of the studies of the velocity fields in the central sources are still ambiguous. It is not clearly established yet, whether or not, the time lags in the response

of the blue and red wings and the core of the line profile with respect to continuum variations are the same. So far, studies of the velocity dependent response of the C IV $\lambda 1549$ emission line in NGC 5548 have found no evidence of significant radial motions in its BLR. (Korista et al. 1995).

Most of the objects, included in the multiwavelength monitoring AGN Watch, are radio-quiet Sy1 galaxies and only one, 3C 390.3 ($z=0.0561$), is a well known broad line radiogalaxy. This type of object represents about 10% of the radio-loud AGNs. It is also a powerful double lobed FRII radio-galaxy with a relatively strong compact core. The two extended lobes, at a position angle of 144° , each one with a hot spot, are separated by about $223''$ (Leahy & Perley 1991). A faint well-collimated thin jet at P.A. = 37° , connecting the core to the northern lobe, has been observed by Leahy & Perley (1995). The VLBI observations at 5 GHz show evidence of superluminal motion (with $v/c \sim 4$) in this parsec scale jet (Alef et al. 1996, 1988).

The strong variability of this object, both in the continuum light and the emission lines is well known (Barr et al. 1980; Yee & Oke 1981; Netzer 1982; Barr et al. 1983; Penston & Perez 1984; Clavel & Wamsteker 1987; Veilleux & Zheng 1991; Shapovalova et al. 1996; Zheng 1996; Wamsteker et al. 1997; Dietrich et al. 1998; O'Brien et al. 1998). The object is also a highly variable X-ray source, with a spectrum showing a broad Fe $K\alpha$ line (Inda et al. 1994; Eracleous et al. 1996; Wozniak et al. 1998). During a multiwavelength monitoring campaign in 1995, several large-amplitude X-ray flares were observed in 3C 390.3; in one of them the X-ray flux increased by a factor of 3 in 12 days (Leighly et al. 1997). Evenmore, Leighly & O'Brien (1997) have presented evidence for nonlinear X-ray variability.

In an analysis of IUE spectra of 3C 390.3, obtained during the 1978–1986 period, Clavel & Wamsteker 1987 detected a variability time lag of 50 and 60 days between the broad emission lines of C IV $\lambda 1549$ and Ly α , and the UV-continuum. However, from a reanalysis of the same spectral data, Wamsteker et al. 1997 have derived a lag of 116 ± 60 days for C IV and 143 ± 60 days for Ly α . Furthermore, from IUE monitoring data for December 1994 to March 1996, O'Brien et al. (1998) obtained a corresponding lag of 35 days for the C IV $\lambda 1549$ emission line and 60 days for Ly α . Yet, from optical monitoring of 3C 390.3 in the 1994–1995 period, Dietrich et al. (1998) derived a time lag of about 20 days for the Balmer lines response to changes in the X-ray continuum. Furthermore, at that time, no temporal lag between the optical and the UV or X-ray continua changes was detected. The UV-bump, usually observed in a large number of Seyfert galaxies is very weak or even absent in 3C 390.3 (Wamsteker et al. 1997). Our object is a prototype of a class that shows very broad, double peaked emission line profiles, to explain this profile, a number of possible scenarios have been suggested. These models contemplate the following hypothetical physical models:

1. Supermassive binary black holes (Gaskell 1983). If each of the black holes (BH) had its own associated BLR, then the blue and red bumps, seen in the broad lines, could be assessed to the corresponding BH. As a result of precession of the binary BH, secular displacements of the peak wavelengths are expected. From the analysis of 3C 390.3 spectra, obtained during 20 years (1968–1988), Gaskell (1996) detected a displacement of the blue bump in H β at +1500 km/s, and determined from the radial velocity changes a possible period of about 300 years that corresponds to $7 \times 10^9 M_{\odot}$ for the BHs. However, Eracleous et al. (1997), having added data on the displacement of the H α blue peak for the 1988–1996 lapse, obtained a period for the binary BH, $P > 800$ years, with an estimated total mass for the binary BH larger than $10^{11} M_{\odot}$. These authors argued that such a large value for the mass of the BH is difficult to reconcile with the fact that, the BHs found so far in the centers of galaxies, have masses lower than $10^9 M_{\odot}$. Therefore, they reject the hypothesis of a binary black hole for 3C 390.3.

2. Outflowing biconical gas streams (Zheng et al. 1991). In this case the response of the broad emission lines to variability of the continuum should occur from the blue wing to the red wing passing through the line core, i.e. the blue and red wings must show different time lags. Although Wamsteker et al. (1997) claimed that the Ly α and C IV $\lambda 1549$ blue wings lagged behind the red ones, implying radial gas motions, this result is not confirmed by Zheng (1996). Apparently, these contradictory results are caused by the rather poor temporal sampling of the UV data (~ 94 days). Dietrich et al. (1998) have not detected any lag in the response of the blue and red wings relative to the core of H α and H β emission. It was also found that the flux in the wings of H β , Ly α and C IV $\lambda 1549$ vary quasi-simultaneously (Shapovalova et al. 1996; O'Brien et al. 1998). These results imply that there are no significant radial motions in the BLR, and Livio & Xu (1997) have shown that the double-peaked lines seen in 3C 390.3 cannot be produced by two line-emitting streams, since the emission region of the far cone jet would be obscured by the optically thick accretion disk.

3. Broad Line emission from an accretion disk in 3C 390.3 has been suggested by Perez et al. (1988). In this case, the emission from an inclined (30°) accretion disk provides a good fit to the broad H α and H β profiles. (Rokaki et al. 1992). Simple disk models predict two symmetrical bumps, the blue bump being slightly brighter due to doppler-boosting effects. However, IUE data shows a blue wing of Ly α much brighter than the red one, this cannot be explained by a doppler boosting effects alone. There are also epochs when the red wing of Ly α is brighter than the blue one (Zheng 1996), i.e. the flux ratio of the red to the blue wings is quite variable. Also, quasiperiodical variations ($P \approx 10$ yr) of the observed flux ratios of the blue and red wings of H β have been reported (Veilleux

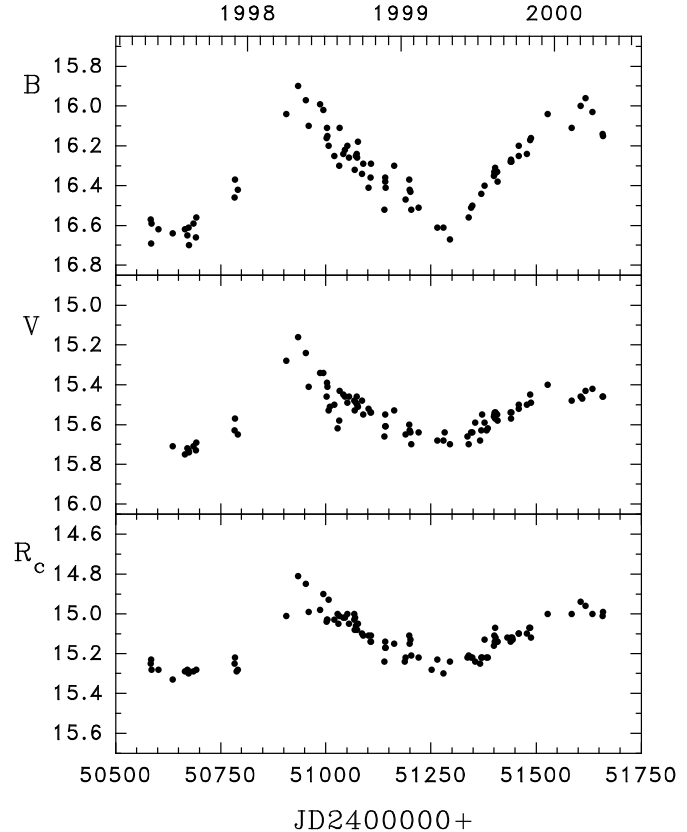


Fig. 1. The light curves of 3C 390.3 in the B,V and R_c photometric bands for a 10 "aperture, in the 1997–2000 period.

& Zheng 1991; Shapovalova et al. 1996; Bochkarev et al. 1997a). In order to explain these variable ratios, more complex models are required; for instance, hot spots (Zheng et al. 1991); two-arm spiral waves in the accretion disk (Chakrabarti & Wiita 1994); or a relativistic eccentric disk (Eracleous et al. 1995).

Long temporal base line studies of the changes in the broad emission line profile through systematic monitoring shall allow us to distinguish between those models.

In this paper, we present the results of the spectral (H β) and photometric BVRI monitoring of 3C 390.3 during the 1995–1999 period. This work is part of the long-term monitoring program for about 10 Seyfert galaxies of different nuclear luminosities started in 1986 at the SAO RAS, and carried out jointly, since 1998, with the INAOE (México), and several observatories in the Former Soviet Union (FSU) and West-European countries (Bochkarev et al. 1997b; Bochkarev & Shapovalova 1999).

2. Observations and Data Reduction

2.1. Photometry

The BVR photometry of 3C 390.3 was carried out at three different observatories i.e. SAO RAS in North Caucasus (Russia), the Crimean Laboratory of the Sternberg Astronomical Institute (CL SAI, Russia) and the Abastumani Astrophysical Observatory (AAO) in Georgia. The observations at the SAO RAS during 1997–2000 were obtained with the 1m and 60cm Zeiss telescopes equipped with an offset guided automatic photometer. The instrument has a liquid nitrogen cooled CCD camera with a format of 1040×1160 pixels, (Amirkhanian et al. 2000). The scale at the CCD being $0.45''$ per pixel, with a corresponding field of view of 7.5×8.5 arcmin. Exposures of the morning and evening sky were adopted as flat-field frames. Bias and dark current frames were also obtained. Data reduction was carried out with the software developed at SAO by Vlasyuk (1993). The photometry is obtained by signal integration in concentric circular apertures, of increasing size, centered at the baricenter of the measured object. The instrumental photometric system of this instrument is similar to those of Johnson in B and V, and of Cousins (1976) in R and I. The VRI photometry during 1998–1999 was obtained at the Crimean Laboratory of the Sternberg Astronomical Institute with the 60cm telescope (Zeiss-600) equipped with an ST-6 thermoelectrically cooled CCD camera. The photometric system of CL SAI is similar to that of Johnson. Further details about SAO and Crimean observations can be found in Doroshenko et al. (2001). BVRI observations at the AAO in Georgia during 1997–1998 were obtained with the 70cm menisk telescope equipped with a CCD camera. These data were reduced with the IRAF package (DAOPHOT). As local photometric standard, we adopted stars “B” and “D” of Penston et al. (1971) which are close to 3C 390.3 in our CCD images. consequently, effects due to differential air mass are negligible for internal calibration purposes. The adopted BVRI magnitudes for the reference stars are given in Table 1.

Table 1. Adopted Photometry for the Standard Stars

Star	B ^a	V ^a	R ^b	I ^b
B	15.04	14.28	14.13	13.59
D	15.40	14.65	14.42	13.90

^aFrom Penston et al. (1971).

^bFrom Dietrich et al. (1998).

The results of the broad-band photometry of 3C 390.3 in the BVR_C filters for a circular aperture of $10''$ obtained at AAO and CL SAI were transformed to the SAO BVR photometric system. Our results are presented in graphical form in Figure 1. The estimated mean errors in the BVRI photometry for the entire data set are 0.026, 0.021, 0.020, 0.022 magnitudes, respectively. In Table 2 our photometric results and the corresponding errors are listed.

Table 2. Photometric Results

Table 2 is only available in electronic form at the CDS via anonymous ftp to cdsarc.u-strasbg.fr (130.79.125.5) or via <http://cdsweb.u-strasbg.fr/Abstract.html>

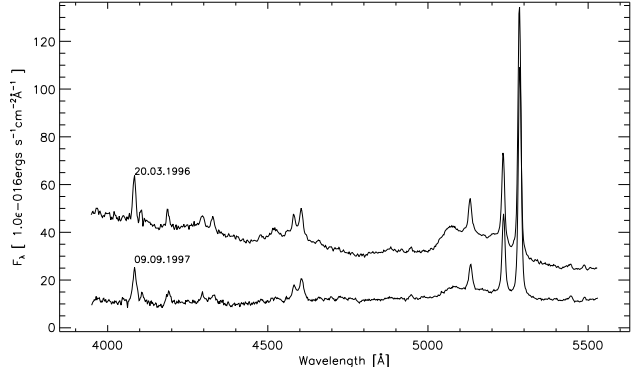


Fig. 3. The spectra corresponding to the high activity (top) and the low activity (bottom) states

The last column lists, the observatory where the data was obtained i.e. (SAO, SAI — Crimean Laboratory, Abast. - Abastumani Astrophysical Observatory in Georgia).

2.2. Optical Spectroscopy

2.2.1. Observations

Spectra of 3C 390.3 were obtained with the 6 m and 1 m telescopes of the SAO RAS (Russia, 1995–1999) and at INAOE’s 2.1 m telescope of the “Guillermo Haro Observatory” (GHO) at Cananea, Sonora, México (1998–1999). The spectra were obtained with long slit spectrographs, equipped with CCD detector arrays. The typical wavelength interval covered is that from 4000 Å to 7500 Å . The spectral resolution varied between 4 and 15 Å . Spectrophotometric standard stars were observed every night. The specific information about the instrumental set-ups in different telescopes is listed in Table 3, there we list: 1 – telescope; 2 – type of focus; 3 – spectrograph; 4 – CCD format; 5 – set-up code. The log of spectroscopic observations is given in Table 4, listed in Cols. 1 – UT date; 2 – Julian date; 3 – code according to Table 3; 4 – projected spectrograph entrance apertures (the first dimension being the slit-width, and the second one the slit-length); 5 – wavelength range covered; 6 – spectral resolution; 7 – seeing; 8 – signal to noise ratio in a region of the continuum (5370 – 5420 Å), where there are no prominent emission or absorption lines. The spectrophotometric data reduction was carried out either with software developed at SAO RAS by Vlasyuk(1993) or with the IRAF package for the spectra obtained in México. The image reduction process included bias, flat-field corrections, cosmic ray removal, 2D wavelength linearization, background subtraction, stacking of the spectra for every set up, and flux calibration.

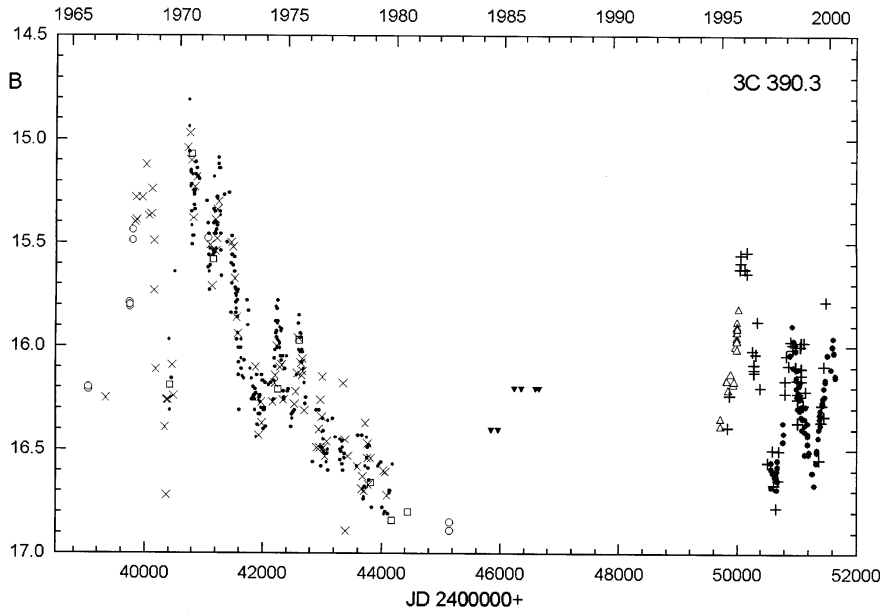


Fig. 2.A A historical light curve for 3C 390.3. Open circles – Sandage (1973), Neizvestny (1986); large filled circles – photometry (present paper); open squares – Yee & Oke (1981); small filled circles – Babadzhanyants et al. (1973, 1974, 1975, 1976, 1984); crosses – Cannon et al. (1971), Scott et al. (1976), Selmes et al. (1975), Pica et al. (1980); pluses – spectral continuum (present paper); open triangles – Dietrich et al. (1998); filled triangles – spectral cont. from Perez et al. (1988) and Lawrence et al. (1996).

Table 3. Characteristics of the telescopes and spectrographs

Telescope	Focus	Equipm.	CCD (pixels)	Code
1	2	3	4	5
6m SAO	Prime	UAGS	530×580	G
6m SAO	Prime	UAGS	1024×1024	P
6m SAO	Prime	MPFS ^a	530×580	T
6m SAO	Nasmyth	Long slit	1024×1024	N
1m Zeiss	Cassegrain	UAGS	530×580	Z1
1m Zeiss	Cassegrain	UAGS	1040×1170	Z2
2.1m GHO	Cassegrain	B&Ch	1024×1024	M

^a MPFS refers to a Multi-Pupil Field Spectrograph

Table 4. Log of the Spectroscopic Observations

Table 4 is only available in electronic form at the CDS via anonymous ftp to cdsarc.u-strasbg.fr (130.79.125.5) or via <http://cdsweb.u-strasbg.fr/Abstract.html>

2.2.2. Absolute Calibration of the Spectra

Since, even under good photometric conditions, the accuracy of spectrophotometric measurements is rarely better than 10%, for the study of AGN's variability the standard scheme for flux calibration by means of comparison with stars of known spectral energy distribution is not acceptable. Instead, we use the flux of the narrow forbidden emission lines which in AGNs are non-variable in timescales of tens of years. This is largely due to the extension of the narrow line emitting region (NLR) and to the lower gas density present in it. Thus, the effects of light traveling through this region, jointly with the long recombination times (t_{rec}) \sim 100 years, for $n_e \sim 10^3 \text{ cm}^{-3}$), damp out the

short time scale variability. Hence, the bright narrow emission lines are usually adopted as internal calibration for scaling AGN spectra (Peterson 1993). However, in the case of 3C 390.3 there has been some discussion about the variability of these lines. Let us address this question in more detail.

From IUE data, Clavel & Wamsteker (1987) found that the flux in the narrow components of Ly α and C IV $\lambda 1549$ emission lines in 3C 390.3 decreased continuously by $\approx 40\%$ between 1978 and 1986. The involved timescales suggest an upper limit of about 10 light years for the size of the regions in which these lines are formed.

Zheng et al. (1995) reported a considerable variability of the [O III] $\lambda 4959$ narrow emission line fluxes (~ 1.8 times) from observations carried out between 1974 and 1990. We believe that this result is somewhat doubtful in the light of the following considerations: the variability is only inferred when comparing results from observations carried out with different instrumental set-ups. They include, on the one hand, fluxes from image dissector scanner (IDS) data, obtained with the Shane 3 m telescope at Lick Observatory through an aperture of $2.8 \times 4''$ (1974–1983 lapse) and on the other hand, observations carried out at La Palma with the 2.5 m Isaac Newton telescope (INT), equipped with an image photon counting system (IPCS) through a $1.6''$ wide slit (1984–1989). The lowest flux values largely correspond to those observed at La Palma through this rather narrow slit. Hence, it is possible that the large differences in flux reported for the [O III] $\lambda 4959$ line could be due to effects associated with the narrow slit used. Evenmore, in the spectra published by Zheng et al. (1995), it is clearly seen that, during 1988 and 1989, the red wing of H β showed an important enhancement and its contribution could have also affected the determination of the [O III] line flux. Unfortunately,

these authors do not provide a detailed discussion of their adopted procedure for flux determination.

Relevant in the context of forbidden line variability are the observations by Yee & Oke (1981) that covered the 1969–1980 lapse, these were carried out with the Hale 5 m telescope using a multichannel spectrophotometer through an aperture of $\sim 10''$. They found that the [O III] lines and the narrow Balmer line fluxes did not change during those years. Furthermore, a detailed study of the [O III] $\lambda 5007$ flux variability in 3C 390.3 was carried out by Dietrich et al. (1998) during 1994–1995. The spectra were obtained through wide apertures ($5'' \times 7.5''$ and $4'' \times 10''$) and were calibrated by comparison with broad band photometry. It was found, as expected, that the [O III] $\lambda 5007$ line flux remained constant (within 2.6%) during the observed time interval. Therefore, we consider that in the case of 3C 390.3 there is no reliable evidence of the [O III] $\lambda\lambda 4959+5007$ flux variability in time scales of months to few years. Our spectra for the $H\beta$ region were scaled by the [O III] $\lambda\lambda 4959+5007$ integrated line flux under the assumption that the latter did not change during the time interval covered by our observations (1995–1999). A value of 1.7×10^{-13} ergs $s^{-1}cm^{-2}$ (Veilleux & Zheng 1991) for the integrated [O III] line flux was adopted. In order to calculate a normalization coefficient, the continuum was determined in two 30\AA wide clean –line free– windows centered at 4800\AA and 5420\AA respectively. After continuum subtraction, blend separation of the $H\beta$ and [O III] components was carried out by means of a Gaussian fitting procedure, applied to the following: $H\beta$ — broad blue, broad red and central narrow; [O III] $\lambda\lambda 4959, 5007$ — broad and narrow components. The forbidden lines are represented by two Gaussian curves with an intensity ratio $I(5007)/I(4959)=2.96$.

2.2.3. Intercalibration of the Spectral Data

The flux of $H\beta$ was determined from scaled spectra after continuum subtraction and removal of the [O III] doublet. The narrow component of $H\beta$ was not subtracted due to possible ambiguities in the fitting scheme for the broad and narrow components of the line. We should mention, that the contribution of the narrow component to the integral $H\beta$ flux is only about 7%. As Peterson & Collins (1983) pointed out, it is necessary to correct the fluxes for aperture effects, due to the fact that while the BLR and nonstellar continuum are effectively pointlike sources ($<1''$), the NLR is an extended one ($>2\text{--}15''$). Then, the measured NLR flux depends on the size of the spectrograph's entrance aperture, and in the case of direct images, on the size of the adopted aperture. The light contribution of the host galaxy to the continuum depends also on the aperture size. Peterson et al. (1995) have shown that the uncertainties in CCD photometry can be minimized, when sufficiently large apertures are adopted. For an aperture of $5'' \times 7.5''$, the expected photometric errors are typically 2 to 3%.

The NLR in 3C 390.3 is more compact than in most Sy1 galaxies, in narrow-band [O III] images, this object shows a compact nuclear emission without signs of an extended structure (Baum et al. 1988). The results of panoramic two-dimensional spectrophotometry of the nuclear region of this object show that the [O III] $\lambda 5007$ emission arises from a zone smaller than $r < 2''$ (Bochkarev et al. 1997a). Furthermore, Osterbrock et al. (1975) obtained a rather low value for the [O III] $F(\lambda 4363)/F(\lambda 5007)$ line ratio, implying a moderately high electron density in the NLR (several $10^6 cm^{-3}$). Since the NLR in 3C 390.3 can be considered as a point source, we did not apply corrections for aperture effects to the nonstellar continuum to narrow line flux ratios or to the broad to narrow line flux ratios, as the light losses in the slit are similar for these components. However, the light contribution to the continuum from the host galaxy does depend on the aperture, and it is necessary to correct this effect. To accomplish this goal, we adopt the scheme by Peterson et al. (1995). Which is based on the ratio:

$$F_{con} = F(4959 + 5007) \left[\frac{F_{con}}{F(4959 + 5007)} \right]_{obs} - G, \quad (1)$$

where $F(4959+5007)$ is the absolute flux in the [O III] doublet and the value in brackets is the continuum to [O III] lines observed flux ratio; G is an aperture dependent correction factor to account for the host galaxy light. Since most of our spectra were obtained with the 6 m telescope through an aperture of $2'' \times 6''$, this instrumental setup was adopted as the standard one (i.e. $G = 0$ by definition). The value of G for the spectra obtained at the 2.1 m telescope (aperture of $2.5'' \times 6.0''$) is $G = 0.046$, while the value obtained for the 1 m telescope (aperture of $8'' \times 19.8''$) is $G = 0.321 \pm 0.028$. In Table 5 we list the derived values of the $H\beta$ flux in the 4990\AA to 5360\AA wavelength range, jointly with the continuum flux at 5125\AA . The mean error (uncertainty) in our flux determination for both, the $H\beta$ and the continuum is $\approx 3\%$. These quantities were estimated by comparing results from spectra obtained within a time interval shorter than 2 days.

In Table 5 we list our results, there we give: 1 – The Julian date; 2 – a code, according to Table 3; 3 – $F(H\beta)$ the total flux (in units of 10^{-13} ergs $s^{-1}cm^{-2}$); 4 – $\varepsilon_{H\beta}$ – the $H\beta$ flux error; 5 – F_c – the continuum flux at 5125\AA (in units of 10^{-15} ergs $s^{-1}cm^{-2}\text{\AA}^{-1}$), reduced to the 6 m telescope aperture ($2'' \times 6''$); 6 – ε_c – the estimated continuum flux error.

3. Data analysis

3.1. A historical B light curve

In order to construct a light curve in the B band dating back to 1966, in addition to our photometric data for the 1997–2000 period, we collected from the literature all the available photometry for 3C 390.3 reported during the last 30 years. We included the photoelectric observations, carried out in 1965–1967, 1971 and 1982 by Sandage

Table 5. Observed H β and continuum fluxes

JD 2440000+	Code	F(H β) [*]	$\varepsilon_{H\beta}$	F _c ^{**}	ε_c
49832.424	G	2.107	0.070	1.309	0.043
49863.375	T	2.715	0.090	1.576	0.052
50039.156	G	2.537	0.084	2.636	0.087
50051.143	G	2.840	0.094	2.703	0.089
50052.149	G	2.368	0.078	2.923	0.097
50127.602	N	3.073	0.101	2.529	0.084
50162.580	N	3.335	0.110	2.571	0.085
50163.553	N	3.502	0.116	2.756	0.091
50249.542	G	2.937	0.097	1.851	0.061
50276.567	G	3.202	0.106	1.638	0.054
50277.556	G	2.961	0.098	1.681	0.056
50281.434	G	2.775	0.092	1.607	0.053
50305.489	G	2.908	0.096	1.813	0.060
50338.319	Z2	2.621	0.087	1.801	0.059
50390.435	G	2.459	0.081	1.592	0.053
50511.622	G	1.761	0.058	1.187	0.039
50599.370	G	1.729	0.057	1.167	0.039
50618.523	G	1.852	0.061	0.996	0.033
50656.499	G	1.585	0.052	0.922	0.030
50691.463	G	1.432	0.047	1.076	0.036
50701.576	N	1.301	0.043	1.160	0.038
50808.582	G	1.718	0.057	1.551	0.051
50813.195	G	1.638	0.054	1.580	0.052
50835.631	N	1.928	0.064	1.799	0.059
50867.560	N	2.080	0.069	1.685	0.056
50904.627	G	1.969	0.065	1.970	0.065
50940.354	N	2.535	0.084	1.832	0.060
50942.342	N	2.531	0.084	1.835	0.061
50990.302	N	2.481	0.082	1.748	0.058
51010.719	M	2.556	0.084	1.582	0.052
51019.723	M	2.544	0.084	1.408	0.047
51023.491	G	2.617	0.086	1.596	0.053
51025.431	G	2.370	0.078	1.408	0.047
51055.376	N	2.313	0.076	1.509	0.050
51074.506	Z1	2.546	0.084	1.537	0.051
51081.429	M	2.250	0.074	1.508	0.050
51082.429	M	2.345	0.077	1.617	0.053
51083.429	M	2.413	0.080	1.570	0.052
51112.259	G	2.339	0.077	1.433	0.047
51130.169	Z1	2.019	0.067	1.705	0.056
51372.516	P	1.610	0.053	1.163	0.038
51410.309	P	1.931	0.064	1.399	0.046
51426.208	P	1.784	0.059	1.393	0.046
51454.674	M	2.223	0.073	1.660	0.055
51455.172	P	2.111	0.070	1.415	0.047
51491.592	M	2.747	0.091	2.321	0.077

^{*} – in units of 10^{-13} ergs s $^{-1}$ cm $^{-2}$ ^{**} – in units of 10^{-15} ergs s $^{-1}$ cm $^{-2}$ A $^{-1}$

(1973) and Neizvestny (1986); spectrophotometric observations for 1970–1979 by Yee & Oke (1981), from which we derived B magnitudes in excellent agreement with contemporary photoelectric photometry. We also make use of the photographic photometry available, ie. 1967–1980 from Cannon et al. (1971); Babadzhanyants et al. (1973;

1974; 1975; 1976; 1984); Selmes et al. (1975); Scott et al. (1976); Pica et al. (1980). In order to increase their accuracy, the photographic observations were averaged in 5 day bins. We also included a few spectral observations by Pérez et al. (1988), Lawrence et al. (1996) and the International Monitoring data in the framework of the AGN Watch consortium for 1994–1995 (Dietrich et al. 1998) and spectral continuum light curve data, discussed here. The resulting light curve in B band is shown in Fig. 2. There, we can see a noticeable increase in luminosity with significant fluctuations between 1965 and 1977. The amplitude of the outburst from the middle of 1969 until the middle of 1970 was about 2 m . In 1979 the brightness of 3C 390.3 decreased to 17 m and remained at this level until 1983. At that time, Penston & Pérez (1984) noted that the broad component of H β had disappeared, and the spectrum of the object became quite similar to that of a Sy2 galaxy. A similar behavior was observed in NGC 4151, for which, after a long lasting photometric minimum between 1984 and 1989 the broad wings of H β also disappeared and was then classified as Sy2 at that time (Penston & Pérez 1984; Lyuty et al. 1984). In the case of 3C 390.3, after maximum light in 1970, on the descending branch of the light curve, important oscillations with an amplitude up to 1 m were observed. Unfortunately, we have not found photometric observations of this object for the 1983–1993 period and hence, the photometric behavior of 3C 390.3 during this period of time is unknown. A detailed study of the character of the visible light variability in 3C 390.3 will be presented in a separate paper.

3.2. Variability of the H β emission line and the optical continuum

The photometric data obtained during 1997–2000 is plotted in fig. 1. The light curve shows an almost sinusoidal change in brightness with a maximum amplitude of about 0 m .8 in the B band. Brightness maxima occurred in May–June 1998 and in March–April 2000. The light curves in the V and R bands are similar in shape to those of the B band, but have a smaller amplitude (\approx 0 m .5), as expected from a blue variable continuum. In fig. 1, one can also notice small amplitude light fluctuations, superimposed on longer time-scale changes. Between 1995 and 1999 the H β flux changes reached a maximum amplitude of 2.7, while those of the continuum at 5125 Å, show a maximum amplitude of \approx 3.2 (Table 5). These changes are evident in a simple inspection of the spectrum of the high-activity state (20 Mar 1996) as compared with corresponding one of the low-activity state (9 Sep 1997). These are plotted in Figure 3. From the combined light curve, (Fig.2). For the 1995–1999 time interval, we confirm a maximum amplitude flux variations in B of \approx 3.2. This value is in excellent agreement with the value derived from spectroscopic continuum fluxes, rendering further support to our basic assumption: ie. that the flux of the [O III] lines did not

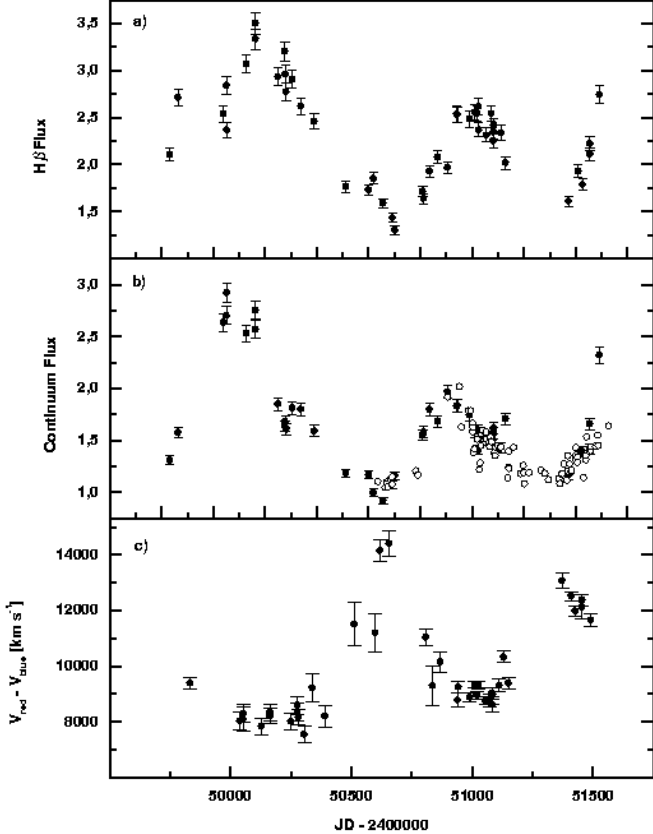


Fig. 4. 3C 390.3 Light curves of the H β panel **a** and the 5125 \AA optical continuum emission panel **b** during 1995–2000. Filled circles represent the spectral data. The photometric points are represented by open circles. Units are 10^{-13} ergs $\text{cm}^{-2}\text{s}^{-1}$ for H β fluxes and 10^{-15} ergs $\text{cm}^{-2}\text{s}^{-1}\text{A}^{-1}$ for the continuum ones. In panel **c** we plot $-V_{\text{red}} - V_{\text{blue}}$, the velocity difference of the red and blue bumps (in km s^{-1}), derived from the H β difference profiles

change during the period of time covered by our observations.

Figures 4a and 4b show the light curves for the integrated H β (4990–5360 \AA) and continuum (5125 \AA) fluxes, these data are given in Table 5. In order to improve the time resolution of our continuum data set, we have added some photometric points in the V band to our spectral continuum data. The V band data was converted into flux adopting the calibration by Johnson (1966). A comparison of the spectral continuum photometry at 5125 \AA ($F_c(5125)$) with 10 simultaneous observations in the V band, yields the following transformation equation:

$$F_c(5125) = (0.941 \pm 0.139) \times F_\lambda(V) - (0.722 \pm 0.326). \quad (2)$$

(correlation coefficient $r = 0.923$). Here the fluxes are given in units of 10^{-15} ergs $\text{cm}^{-2}\text{s}^{-1}\text{A}^{-1}$).

In Figures 4a and 4b two outbursts in H β and the continuum are evident, with time intervals between minima of ≈ 1000 days (Oct. 1994 – Jul. 1997) and ≈ 700 days (Jul. 1997 – Jun. 1999), respectively. Also, the presence of

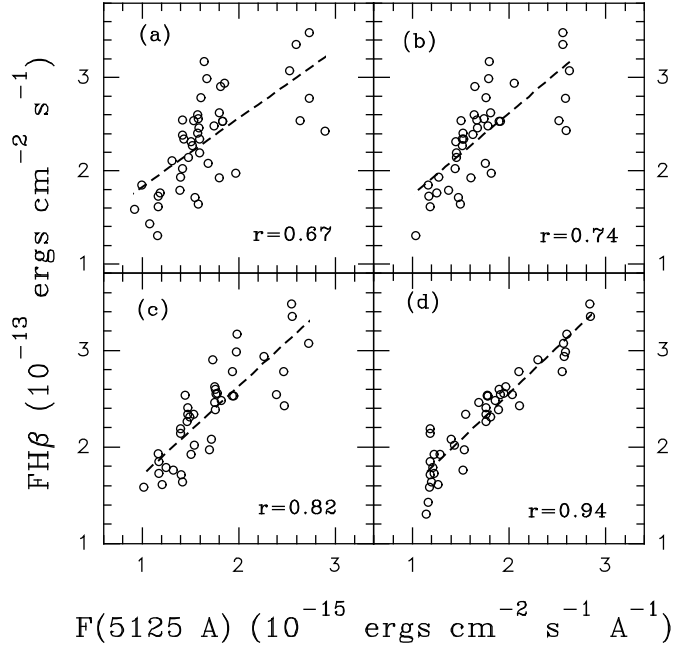


Fig. 5. The $F(\text{H}\beta)$ and $F_c(5125)$ plotted against each other. In panels a, b, c & d these quantities are plotted taking into account a time lag of 0, 20, 40 and 100 days, respectively. The correlation coefficients for the linear regressions are also given.

a time lag between the continuum light changes and the response of the H β line, is also noticeable.

Fig. 5a,b,c,d shows the observed correlation between the continuum and H β light curves, for a time lag between the continuum and line variations of 0, 20, 40 and 100 days respectively. There, it is clearly seen that the variance of the data is minimal while the correlation coefficient is maximal ($r=0.94$) for a delay of 100 days. In latter case, we obtain the following relationship:

$$F(\text{H}\beta) = (0.957 \pm 0.056) \times F_c(5125) + (0.640 \pm 0.102) \quad (3)$$

Here $F_c(5125)$ fluxes are expressed in units of 10^{-15} ergs $\text{cm}^{-2}\text{s}^{-1}\text{A}^{-1}$ and the $F(\text{H}\beta)$ fluxes in units of 10^{-13} ergs $\text{cm}^{-2}\text{s}^{-1}$. The values chosen for the delays are typical values previously mentioned in the literature. In Sect. 3.4 we present a detailed discussion of the delays from a cross-correlation analysis of our data.

3.3. The H β wings

In order to investigate the flux in the different parts of the H β profile, we studied three different velocity bins: a blue wing (-7100 km s^{-1} to -1900 km s^{-1}), a core (-1900 km s^{-1} to $+1900 \text{ km s}^{-1}$) and a red wing ($+1900 \text{ km s}^{-1}$ to $+7100 \text{ km s}^{-1}$). The light curves for these are presented in Figures 6 a,b,c, there, we can see that the changes in both the blue and red wings and the core occur quasi-simultaneously. This fact implies that, there are predominantly circular motions in the region where the broad H β emission originates. The blue-to-red wing flux ratio

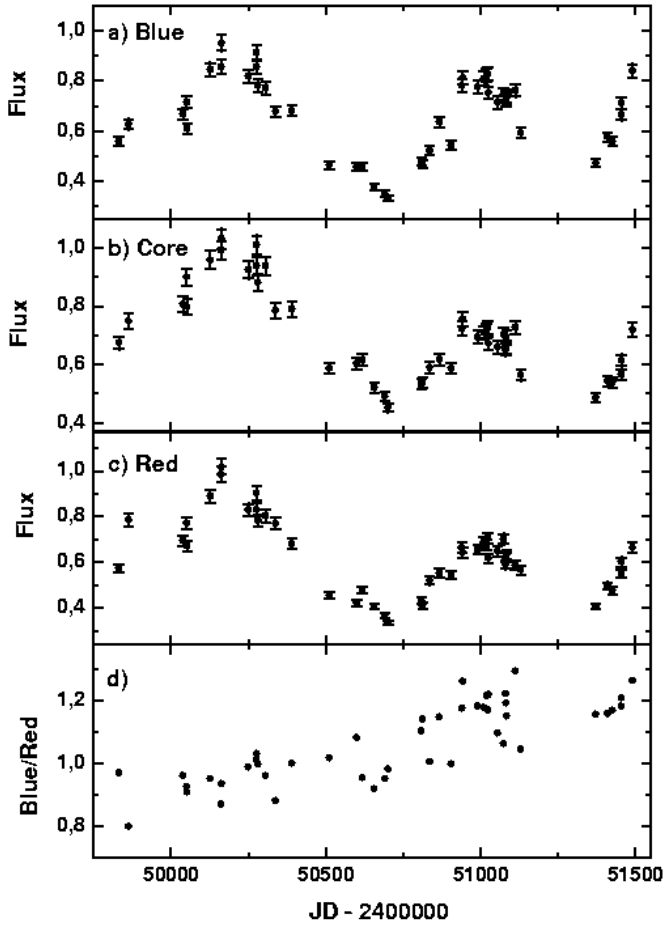


Fig. 6. The light curves. (a)-(c) for the blue wing in the 5010–5099 Å (-7100 km s^{-1} to -1900 km s^{-1}), interval, for the core in the 5099–5164 Å (-1900 km s^{-1} to $+1900 \text{ km s}^{-1}$), interval, and for the red wing of H β emission line in the 5164–5253 Å ($+1900 \text{ km s}^{-1}$ to $+7100 \text{ km s}^{-1}$), interval, respectively. Panel (d) shows the temporal behavior of the the blue-to-red wing flux ratio R

R is also shown in Fig. 6d. Veilleux & Zheng (1991) noticed that between 1974 and 1988, the blue-to-red wing flux ratio followed a fairly smooth, almost sinusoidal pattern with an apparent period of 10.4 yrs. This trend was confirmed by Bochkarev et al. (1997a) with observations that extended until 1995. Although maxima for the ratio R were observed in the years: 1975, 1985, and 1995, the sinusoidal trend of R did not continue during the 1996–1999 period. In Fig. 6d, it is evident that R continued to increase in a nearly monotonic fashion between 1995 and 1999.

3.4. Cross-Correlation Analysis

3.4.1. The CCF of the H β broad and continuum emissions

In order to determine a more accurate time lag than the one described in 3.2, we carried out a time series analysis using the cross-correlation function (CCF). The CCF was

calculated by means of the interpolation method described by Gaskell & Sparke (1986) and White & Peterson (cite-whi). We computed both the lags related to the CCF peak (t_{max}) and the CCF centroid (t_{cen}). The value of (t_{cen}) is that of the center of mass of the CCF for positive delay values. The CCF is calculated by pairing each of the real data points in both time-series with linearly interpolated points for any arbitrary time delay.

According to Gaskell and Peterson (1987) not every time series is suitable for the cross-correlation analysis, only those series, for which the autocorrelation function (ACF) width is wider (by at least 10%) than the width of the corresponding function for the sampling window (ACFW), contain relevant information about time lags. The ACFW is computed by repeated sampling of white noise light curves, convolved with the observational window. This procedure provides a measure of how much of the width of the ACF is due to the interpolating scheme, instead of the real correlation width of a continuous time series sampled at discrete times. In addition, the half width of the ACF at a zero correlation level determines the characteristic size of the region from which variations originate, setting an upper limit to the **BLR** size.

The ACFW was calculated for the time series of the observations, upon which, random Gaussian noise corresponding to the observing errors in the time series was superimposed. The mean ACFW for one hundred of those realizations is shown in Fig. 7a. There we can see that the ACFW is much narrower than the ACF for either the continuum or the H β emissions.

Usually, the time delay is determined either by the location of the peak, or that of the center of mass of the cross-correlation function between the continuum and the emission line light curves. Robinson and Pérez (1990) argued that the position of the CCF peak (t_{max}) yields the time delay corresponding to the inner radius of the **BLR**, while the position of the center of mass of the CCF (t_{cen}) relates to the size of the **BLR** weighted by luminosity.

The errors, in the determination of the time lags, were estimated through a Monte Carlo simulation. From 1000 independent realizations of the CCF, the t_{max} and t_{cen} distributions were obtained. Prior to the computation, the time-series involved, were corrupted with Gaussian noise in correspondence to the typical errors in them. Cutting the distribution functions at a 17% probability level, the uncertainty related to a 67% confidence level (1σ error) was determined.

Given that, during the International Monitoring Programme of the Sy galaxy NGC 5548, for a period of 8 years, it was observed by Peterson et al. (1999) that the time lag in this object does not have a constant value, and that changes of the delay may be related to the luminosity variations of the central source. And since, during time interval cover by our observations, the photometric and spectral light curves of 3C 390.3 show two distinct flares. It is important to determine the delays not only for the entire time-series, but also for the segments of it, that correspond to relevant events in the

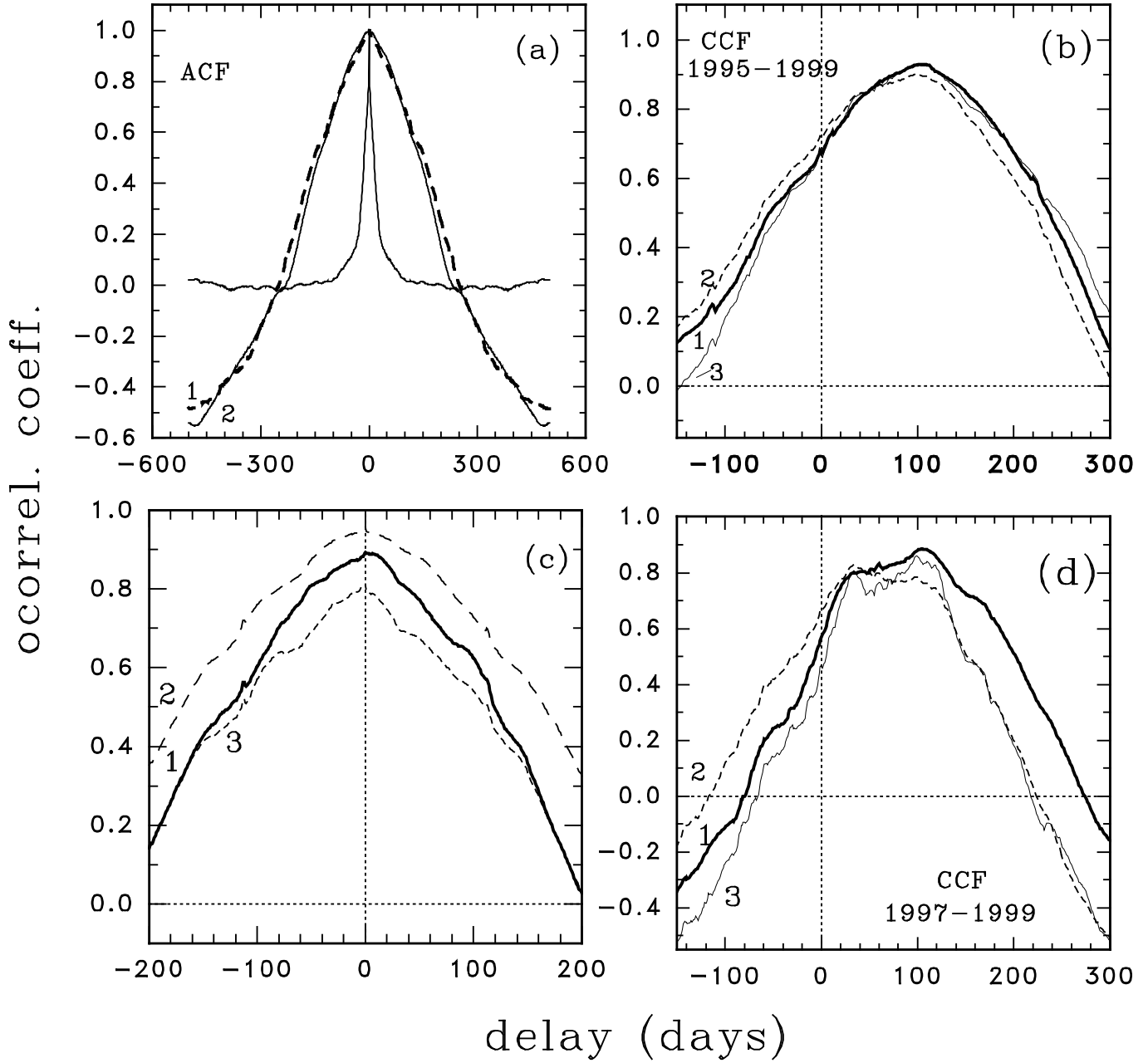


Fig. 7. The Auto- and Cross-Correlation Functions. In panel (a), the narrow curve represents the sampling window autocorrelation function (ACFW) for the spectral continuum and H β line. Also, the autocorrelation functions (ACF) for the H β label (1) - and the continuum light curves (2) are shown. On panels (b) and (d), the CCFs for the periods 1995-1999 and 1997-1999 respectively are shown. Curves label (1) represent the CCF between the H β flux and the spectral continuum at 5125Å; curves labeled (2) represent the CCF for the H β flux and the combined continuum and label (3) refers to the CCF computed as in case (2), but for a restricted interpolation of 100 days. Panel (c) shows the CCF between: (1) - H β blue and red wings light curves , (2) - H β red wing and H β core fluxes and (3) - H β blue wing and H β core light curves. In every panel the units are: delay in days (abscissae) and correlation coefficient (ordinates).

light curves. Therefore, analysis of the light curves was carried out for various cases, as follows:

The CCF analysis has been carried out separately for the entire data set – case A (JD=2449832-2451527), and for the two sub-sets (case B, JD=2449832-2450701; and case C JD=2450618-2451527). It should be mentioned

that for case B, we do not have supplementary photometry. While in case C we have included our broad band photometry. For this reason, the flux cross-correlation was calculated not only for the spectral continuum fluxes F_{sc} , but also for the combined continuum data F_{scv} . To the

latter, we added our photometric data in the V band to the spectral continuum data as discussed above in 3.2.

Since many spectral observations were obtained with long time intervals between them, the CCF was calculated restricting the interpolation processes to time intervals no longer than 100 days (cases - AD, CD). That is, prior to the CCF computation, both time series were analyzed as to whether or not they were suitable for pairing. With this 100 day restriction in the pairing, possible effects associated to long time gaps are reduced.

The results of the cross-correlation analysis are presented in fig. 7 and summarized in Table 6. There we list: in Col. 1 the time-series case; in col. 2 – the cross-correlation case: $(F(H\beta) - F_{sc})$ – between the continuum flux $F(5125)$ and $H\beta$ flux; $(F(H\beta) - F_{scv})$ – between the combined continuum flux $(F(5125) + F(V))$ and $H\beta$ flux; in col. 3 – t_{max} – the time lag in days, determined from the position of the CCF maxima; in col. 4 – 1σ interval for t_{max} ; in col. 5 – r_{max} – the cross-correlation coefficient for the CCF maxima; in col. 6 – t_{cen} – the time lag in days, determined from the centroids of the CCF; in col. 7 – the estimated 1σ uncertainty for t_{cen} ; in cols. 8 and 9 – the number of points, used in the computations – $N(H\beta)$ and – N_c .

Inspection of Fig. 7 and Table 6, shows that:

1. All cases yield a time lag of $H\beta$ relative the continuum flux changes $t_{max} \approx 100 \pm 10$ days or a little less for $t_{cen} \approx 90 \pm 10$ days.
2. In the time interval from Jun.1997 - Dec. 1999 (case C), an additional, shorter delay of 33-37 days is apparent.

Our delay values differ from the results of Dietrich et al.(1998). From Fig. 5 one can clearly see, that the 20 day lag, obtained by these authors yields a much larger variance and lower correlation coefficient between line and continuum fluxes than the 100 day lag. In our data we do not see a lag of 20 days or something like it. The reason of this discrepancy is not clear to us. Perhaps it is related with the longer time interval covered by our observations. It is conceivable that the time delay in this object does not have a constant value, and that changes of the time lag may be related to the luminosity variations of the central source. A similar case to that of the Sy galaxy NGC 5548 studied by Peterson et al. (1999).

3.4.2. The CCF for different parts of the $H\beta$ profile

We calculated the cross-correlation of the responses of the blue wing (-7100 to -1900 km/s), of the core (-1900 to $+1900$ km/s) and of the red wing ($+1900$ to $+7100$ km/s) of the $H\beta$ profile to variations of the optical continuum. The delays found were 100–113 light days for t_{max} , and 86–102 light days for t_{cen} . However, it should be mentioned that 7% of the maxima in the distribution of the CCF peak for the case of the $F(H\beta)$ blue wing – F_{scv} correspond to a delay of about 40 days, almost the same as in case C previously discussed (see Sect. 3.4.1).

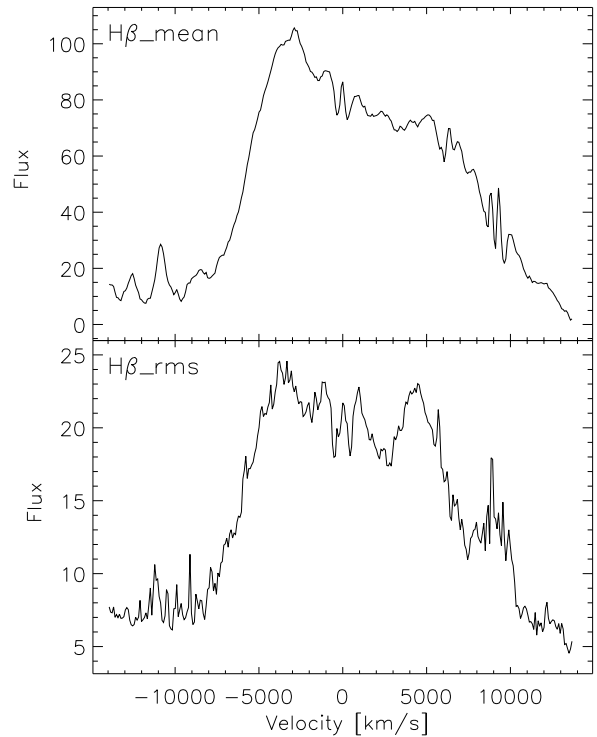


Fig. 9. The mean and rms $H\beta$ profiles in velocity units

The possible differences in the response of the various parts of the line profile can be studied through their cross-correlation functions. In our case, the cross-correlation of the blue-core, red-core and blue-red $H\beta$ components are presented in Fig. 7c. The corresponding time lags for the blue and red wings relative to the core, and of the wings relative to each other are listed in Table 6. There, we can see that our CCF analysis for the $H\beta$ wings does not reveal any delay in the variations of the line wings with respect to the central part of the line, or relative to each other. These results preclude the possibility of having a BLR velocity field dominated by radial motions.

3.5. $H\beta$ profile changes

In Fig. 8, we present the profiles of the broad $H\beta$ component, in velocity units relative to the narrow component. There the narrow [O III] and $H\beta$ emissions were removed by means of the Gaussian-fit procedure previously described. Characteristic features in the profile of the broad $H\beta$ line are the presence of a blue bump and an extended red wing. The blue wing of $H\beta$ was brighter than the red one during the 1995–1999 interval. In 1996, the intensity of the wings was very strong. Yet in 1997, the emission in the $H\beta$ wings was rather weak.

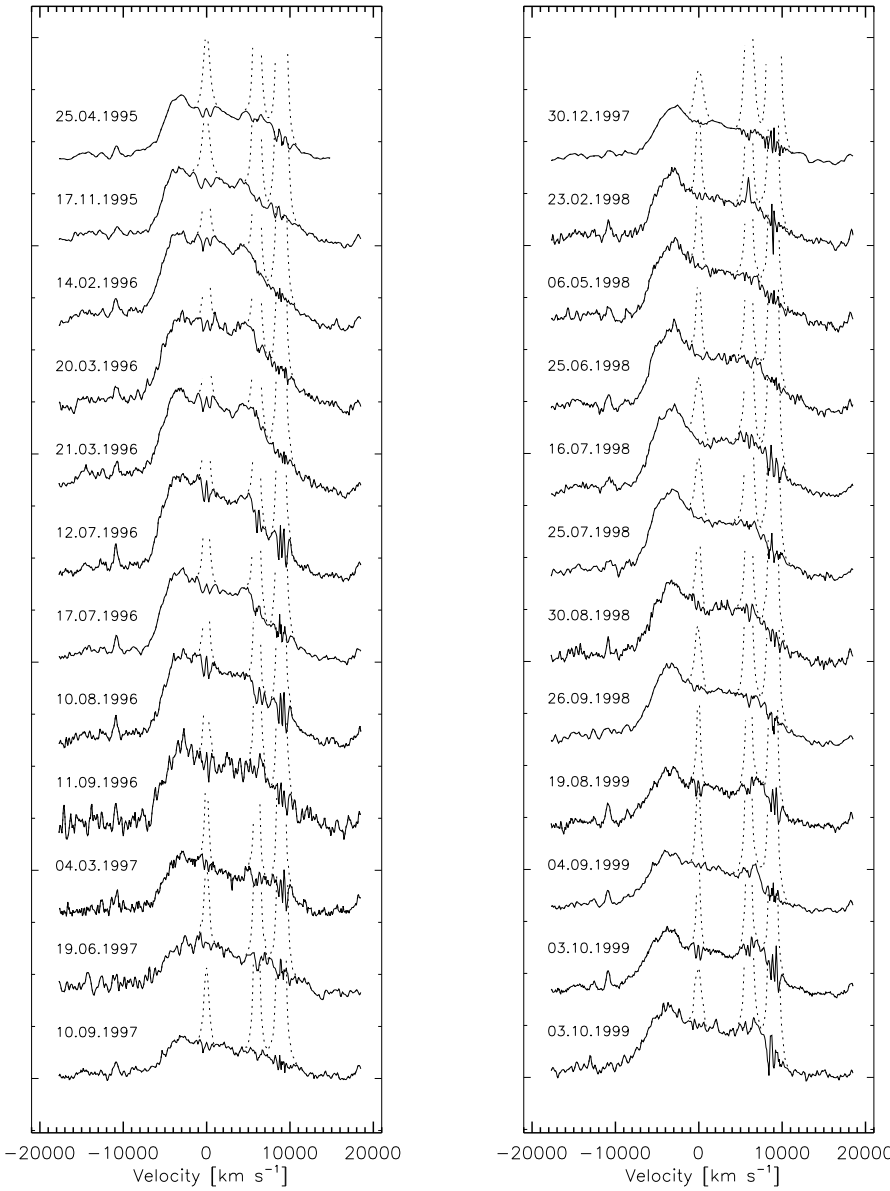


Fig. 8. Typical broad $H\beta$ profiles (solid line) after continuum and narrow components subtraction (dashed line).

3.5.1. Mean and Root-Mean-Square Spectra

The comparison between the average and root-mean-square (rms) spectra provides us with a good measure of profile variability. Since, any constant contribution to the spectra is excluded from the rms spectrum. The mean $H\beta$ profile after removing narrow the $H\beta$ and $[O\text{ III}]$ lines and the absolute rms variations per unit wavelength are shown in Fig. 9. Our results are similar to those of Dietrich et al. (1998): ie. the mean $H\beta$ profile is clearly asymmetrical with a full width at zero intensity of about 20 000 km s^{-1} . The blue bump in the mean spectrum is located between -3000 and -4000 km s^{-1} while the red bump is seen between +4000 and +5000 km s^{-1} . The mean profile shows a blue bump brighter than the red one during the

1995–1999 lapse. From Fig. 9 (bottom) the FWHM-(rms) is about 12 000 km s^{-1} .

3.6. The velocities of the $H\beta$ blue bump

We have measured the radial velocities of the emission peak of the $H\beta$ blue bump relative to the narrow $H\beta$ component from Gaussian fits of the top of the blue bump down to the 30% level of the peak brightness. A method similar to that applied by Eracleous et al. (1997). A comparison of our blue bump radial velocities with theirs, for the same epochs show a very good agreement between both sets of observations. The mean difference being about $\pm 60 \text{ km s}^{-1}$, a value close to the uncertainties of the procedures adopted. Our results are presented, in graphic form (open circles), in Figure 10. Each point represents an av-

Table 6. Time Delays in Days

Time series	Case	t_{max}	1σ interv.	r_{max}	t_{cen}	1σ interv.	$N(H\beta)$	N_c
A	$F(H\beta)-F_{sc}$	105		0.928	99		44	44
A	$F(H\beta)-F_{scv}$	100	97–101	0.900	86	79–92	44	127
AD	$F(H\beta)-F_{scv}$	99		0.930	98		37	45
B	$F(H\beta)-F_{sc}$	98		0.946	109		20	21
B	$F(H\beta)-F_{scv}$	99	93–113	0.954	112	98–114	20	29
C	$F(H\beta)-F_{sc}$	105		0.885	90		27	26
		34		0.800				
C	$F(H\beta)-F_{scv}$	34	33–37	0.829	63	50–72	27	109
		99	97–119	0.784				
CD	$F(H\beta)-F_{scv}$	99		0.859	78		24	33
		33		0.803				
A	$F(H\beta)b-F(H\beta)c$	0	-3.7–1.2	0.809	-1.6	-5.0–1.2	44	44
A	$F(H\beta)r-F(H\beta)c$	-1.0	-3.3–0.9	0.957	-1.5	-4.6–0.8	44	44
A	$F(H\beta)b-F(H\beta)r$	0.5	-1.3–7.8	0.894	0.6	-2.1–8.0	44	44

verage of several spectra obtained during a lapse of a few months. The absolute value of the radial velocity of the blue bump presents a minimum, observed in 1997, at $\approx -2900 \text{ km s}^{-1}$, and a maximum occurring in October 1999 at $\approx -3700 \text{ km s}^{-1}$. The velocity shift of the blue bump reached a value of about 800 km s^{-1} during this time. The changes of the blue bump velocity between 1967 and 1999, taken from the literature, are also presented in Fig. 10. The short dashed line represents the best fit of the double-line spectroscopic binary model by Gaskell (1996), while, the long dashed line represents the fit by Eracleous et al. (1997). One can see that our data are reasonably well described by the latter. These authors have shown that, if the displacement of the blue bump peak velocity originated from individual broad-line regions, associated with a massive binary BH, then the inferred rotation period would be about 800 years, and the associated mass would then be larger than $10^{11} M_\odot$. This value for the BH mass is much larger than the expected by comparison with other BH candidates found at the center of galaxies. Therefore, these authors rejected the binary BH interpretation. Our results further support their conclusions.

3.7. The H β difference profile

We obtained the H β difference profiles by subtraction of the minimum-activity average spectrum (9 September, 1997) from individual spectra. This is done after continuum, narrow H β and [O III] emission had been subtracted as well. When the spectra for subsequent nights, presented small differences i.e. H β integral flux remained constant within 3 to 5%, they were averaged and the spectra of low signal to noise ratio ($S/N < 20$) were excluded from the analysis. The annual average differential profiles of the broad H β line are shown in Fig. 11. In order to determine the blue and red peak velocities, the mean difference profiles were fitted with three Gaussian functions; one to the blue bump, one to the core, and one to the red bump. The derived differences, of the peak velocity for the red and blue

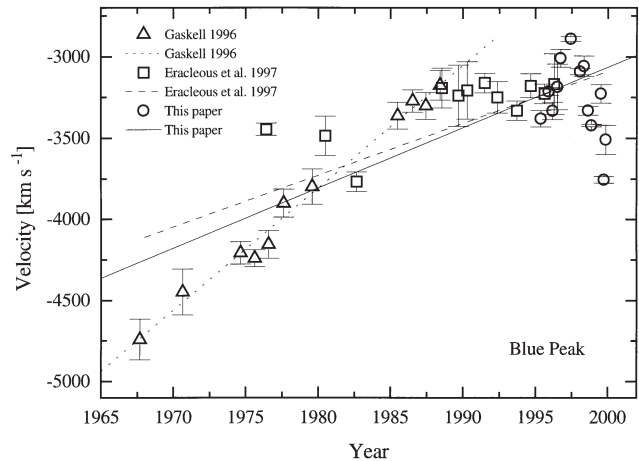


Fig. 10. The average radial velocity curve of the blue bump peak. The different symbols represent: triangles – the annual H β average data from Gaskell (1996), open squares – the H α data from Eracleous et al. (1997), open circles – our H β data. The different best fit models are explained in the top left panel.

bumps, $V_r - V_b$, are plotted in Fig. 4 c. Despite the errors in the determination of the velocities, a distinct anticorrelation is observed between the difference $V_r - V_b$ and the flux changes in both H β and continuum emission, as it is clearly seen in Fig. 4.

The annual mean velocity of the blue, red and core components derived from the Gaussian analysis, jointly with the $V_r - V_b$ velocity difference of the bumps, are listed in Table 7. There we notice that, the radial velocity of the blue component increased in absolute value from -3200 km s^{-1} in 1995–1996 to -5200 km s^{-1} in 1999. At the same time the radial velocity of the red component increased from $+4900 \text{ km s}^{-1}$ in 1995–1996 to $+7000 \text{ km s}^{-1}$ in 1999. Then, the absolute velocity of both components increased by about 2000 km s^{-1} during this period of time. That is, the difference $V_r - V_b$ increased by about

Table 7. Radial velocities of the blue bump, red bump and core of H β derived from the difference profiles, jointly with contemporary H β fluxes.

Velocity (km s $^{-1}$) Fluxes	Time Interval			
	Apr.1995-Nov.1996	(Mar.-Aug.)1997	(Jan.-Oct.)1998	(Jul.-Oct.)1999
V _{blue}	-3204 \pm 187	—	-3867 \pm 75	-5215 \pm 118
V _{red}	4899 \pm 155	—	5361 \pm 134	7001 \pm 106
V _{core}	617 \pm 187	76 \pm 249	335 \pm 235	1170 \pm 244
V _r -V _b	8103 \pm 243	—	9228 \pm 154	12216 \pm 158
F(H β) [*]	2.804 \pm 0.37	1.733 \pm 0.14	2.367 \pm 0.21	1.932 \pm 0.25
F _{con} ^{**}	2.132 \pm 0.54	1.035 \pm 0.13	1.611 \pm 0.14	1.406 \pm 0.17

* – in units of 10 $^{-13}$ ergs s $^{-1}$ cm $^{-2}$

** – in units of 10 $^{-15}$ ergs s $^{-1}$ cm $^{-2}$ A $^{-1}$

4000 km s $^{-1}$. Table 7 lists the observed mean fluxes of H β (F(H β)) and continuum (F_{con}) light in the same time intervals. It is evident that the lower annual average velocities of the blue and red components, or their difference correspond to larger mean flux values. In the frame of an accretion disk model, the optical continuum changes are a consequence of changes of the luminosity of the central X-ray source, causing a variable disk irradiation.

The observed velocity variations could be explained if, at different times, the zone that contributes with the maximum luminosity to H β , changes in radius within the disk. The position of this zone will depend on the luminosity of the central source. Then, it is likely that during 1995–96, we were observing enhanced H β emission from parts of the disk which are located further away from the BH ie, when the luminosity of the central source is higher, and consequently heated the outer regions of the disk. This results in a maximum emission zone located at larger disk radii. Later on, in 1999, maximum emission came from parts of the disk located at a smaller radii, when the luminosity of the central source was much lower. In the case of a circular disk the ratio of the maximum H β emission radii must be proportional to the inverse squared velocity. Hence, if we consider the velocity values listed in Table 7 for 1995–96 and the average velocity values for 1998–99, the ratio of the radii of maximum H β emission is about 1.77 \pm 0.2. This is in excellent agreement with the ratio of the size of the emitting zones as inferred from the lag time ratio of the centroids of the CCF (ie. 1.78 \pm 0.3, see Table 6).

These transient phenomena are expected to result from the variable accretion rate close to the central black hole. Note that from the theory of thin accretion disks (Shakura & Sunyaev 1973) one can calculate the energy dissipated through viscosity, the resulting spectrum emitted by the disk, and time scales in which, the emission from the disk varies in response to a variable accretion rate. These are rather long (\approx 10 5 years for a 10 7 M \odot BH). However, as the accreted matter approaches the BH, at a distance of few tens of gravitational radii, a large fraction of the accretion energy is transformed into X-ray radiation. The rapid variability of this radiation on time scales of hours,

days and weeks is due to changes in the final accretion rates.

Currently, a model in which the surface temperature of the disk is modulated by the irradiation caused by a variable luminosity of the X-ray source has been suggested by several authors (see Ulrich, 2000 and references therein). In some models it is assumed that the rapid variability (days, weeks) of the continuum X-ray source can be explained by the fact that a significant fraction of the accretion energy near the black hole is spent on heating a corona by a mechanism reminiscent of flares in the solar corona (Galeev et al. 1979). Hot electrons, in turn, transfer some of their energy to ambient soft X-ray and UV photons (some emitted by the disk), producing medium energy and hard X-ray radiation via inverse Compton emission.

3.8. Modeling of the H β Broad Components

As mentioned above, several models have been proposed to explain the double-peaked line profiles. Among them, the emission by an accretion disk or a torus, whose presence seems essential to fuel a black hole. Our study favours the formation of the broad H β line of 3C 390.3 in an accretion disk. Superluminal motions have been observed at radio frequencies (Alef et al. 1996), these are indicative of the presence of a relativistic jet, with its axis aligned close to the line of sight (Orr & Browne, 1982). Therefore, the disk's axis is probably close to the line of sight.

Under the assumption of an accretion disk as the site of emission line formation, the study of the profile changes with time, may provide relevant information, even if we do not advance any hypothesis about the disk structure or to how it is illuminated. Moreover, we could reject the disk hypothesis, if we find some inconsistency in the results (for instance a change of the BH mass or the disk inclination).

We assumed that: i) the Balmer lines are emitted by a disk rotating about a central object with Keplerian velocity, and ii) the disk emissivity varies with the distance $r = R/R_g$ to the center, where R_g is the gravitational radius (2GM/c 2) with M being the mass of the BH. Then we computed the profiles emitted by such disk, taking into ac-

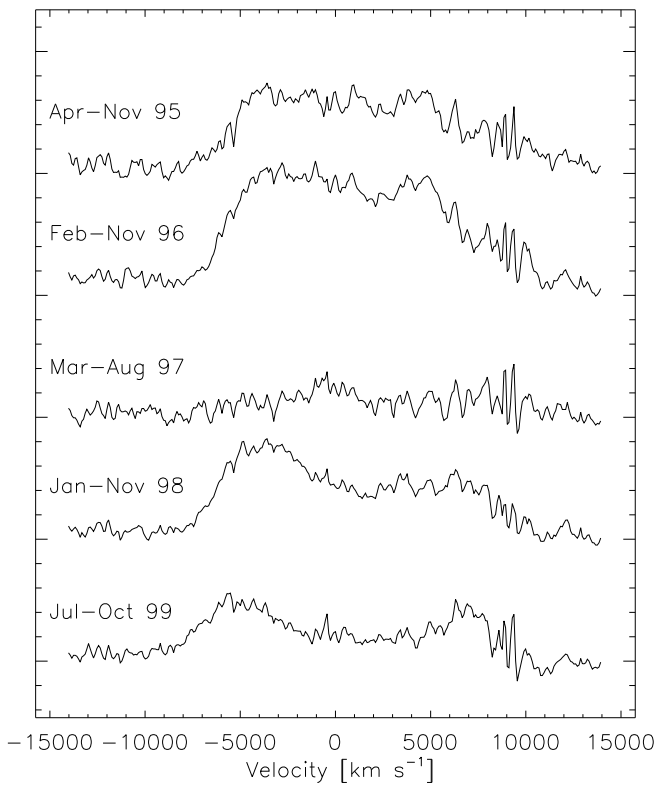


Fig. 11. Annual averages from 1995 to 1999 of the difference profiles for the broad H β line.

count the relativistic Doppler and gravitational redshifts, using the equations given by Gerbal & Pelat (1981) and Chen et al. (1989). These equations are valid for a disk seen at inclination angles i smaller than 80 deg, which is the case for 3C390.3. The resulting profiles are double-peaked and asymmetric. They were convolved with the instrumental profiles and fitted to the observed ones, using the Davidon-Fletcher-Powell method found in Minuit's package (James 1994).

One important parameter in the fitting procedure is the inclination angle i , which must remain constant. For a simple power-law for the disk emissivity ie. $F(\text{H}\beta) \propto r^{-q}$, the line wings cannot be properly reproduced, a fact already noticed by Chen et al. (1989) for Arp 102. The profile fits are improved significantly, when a double power-law emissivity function is adopted. In this case, the important fitting parameters of the model are: the indices q_1 and q_2 , the radius r_1 at which the slope changes from q_1 to q_2 , and the outer radius of the disk, r_{out} (all radii being expressed in units of R_g). The inner disk radius does not play an important role. The four relevant parameters are expected to vary with the continuum flux level and the illumination of the disk.

In this paper, we present only a few of the results, a more detailed description of the model and the results for the H α and H β profiles will be presented in a separate paper.

The fits of four selected H β profiles, distributed in time, and representative of maximum and minimum activity states, are shown in Fig. 12. From our fitting procedure we find that: i) $i = 25 \pm 3$ degrees, consistent with a constant value of i , and ii) surprisingly, despite the large changes in the continuum and line fluxes, $q_1 \approx 1$ and $r_1 \approx 200R_g$ do not vary significantly, while q_2 varies between 3.46 and 3.51 for the fits to the four profiles.

One should seek a physical explanation of this behavior. According to the results, the bulk of the line emission is produced at a radius close to r_1 i.e. at $R \approx 200R_g$.

It is interesting to note that this value corresponds to the radius where the accretion disk becomes gravitationally unstable (cf. Collin & Huré 2001). At larger radii, the emissivity decreases very rapidly, faster than it would be expected in the case a continuum source illuminating the accretion disk, or a system of rotating clouds having a constant density with a canonical BLR value of $n \geq 10^9 \text{ cm}^{-3}$. In this case, $F(\text{H}\beta)$ would roughly be $\propto F_{inc}^{0.5}$ (cf. for instance Dumont, et al. 1998), where F_{inc} is the flux incident on the disk. And since at large distances from the continuum source $F_{inc} \propto r^{-3}$, one would find that $F(\text{H}\beta) \approx r^{-1.5}$ for a constant density. If the disk is geometrically thick (a "torus"), the exponent is smaller, F_{inc} being proportional roughly to r^{-2} . This means that the density decreases rapidly with increasing radius, as about r^{-2} , as expected if the disk is in a state of marginal instability (Collin & Huré, 1999). On the other hand, for smaller radii, the emissivity varies slowly with r , which is compatible with the disk irradiated by the central source of continuum if the density is larger than 10^9 cm^{-3} . Thus this simple change of the density in the accretion disk could induce a "physical radius" of the emission region quite independent of the value of the continuum flux, and could explain why the radius of maximum emission does not vary strongly during the monitoring.

So, our study favours the formation of the broad H β line of 3C 390.3 in an accretion disk.

3.9. The mass of the Black Hole in 3C 390.3

Using the virial theorem jointly with the reverberation-rms method (cf. Peterson et al. 1998), the mass of the black hole in 3C390.3 can be estimated from the relationship of Wandel et al., (1999):

$$M_{rev} \approx (1.45 \times 10^5 M_{\odot}) \left(\frac{c\tau}{\text{lt - day}} \right) v_{rms,3}^2, \quad (4)$$

where $v_{rms,3} = v_{FWHM}(\text{rms})/10^3 \text{ km s}^{-1}$.

Using our results: $v_{FWHM}(\text{rms}) \approx 12000 \text{ km s}^{-1}$ (Fig. 9b), $(c\tau/\text{lt - day}) \approx 100$ (Table 7), we obtained $M_{rev} \approx 2.1 \times 10^9 M_{\odot}$. This value is substantially larger than $M_{rev} \approx 4 \times 10^8 M_{\odot}$, obtained by Wandel et al. (1999). The difference is due to the fact that the determination of Wandel et al. is based upon: 1) a time lag of 24 days, instead of the 100-day lag found in the present study; 2) a the value for $v_{FWHM}(\text{rms}) \approx 10500 \text{ km s}^{-1}$

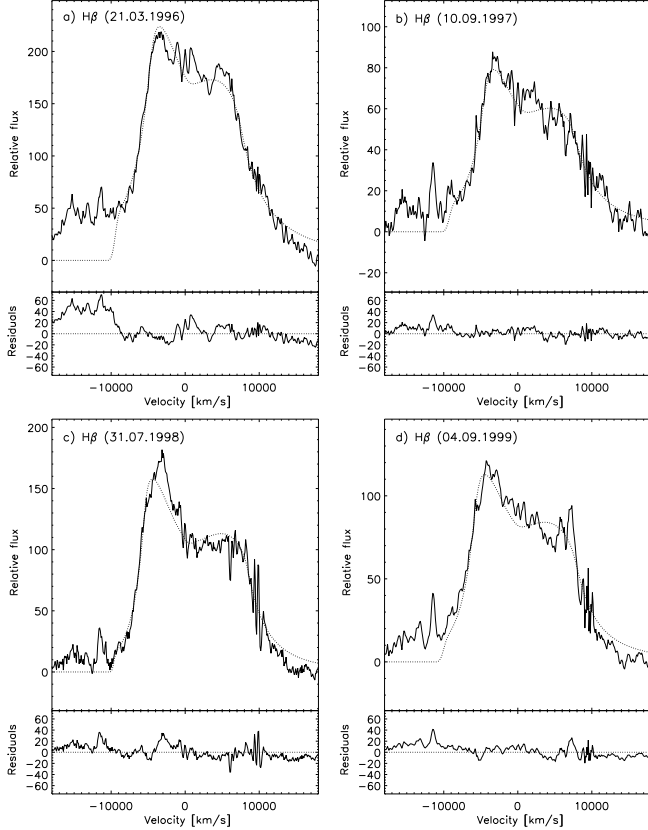


Fig. 12. The fits to the $H\beta$ observed profiles for different epochs, by an accretion disk model with an inclination angle of about 25° , and with a region of maximum emission at about 200 gravitation radius. The dotted line represents the model profile, while the full thin line the observed one. In each window, the lower panel represents the residuals for the following dates: JD=24410163, 24410701, 24411025, 24411426.

instead of our value for $v_{FWHM}(\text{rms}) \approx 12000 \text{ km s}^{-1}$. The upper limit for the mass of the BH in 3C 390.3, estimated from X-ray variability is $M(\text{BH}) < 1.5 \times 10^{10} M_\odot$ (Eracleous et al. 1997).

Assuming that $M_{rev} \approx M(\text{BH})$, we estimate a value for R_g (the BH gravitational radius), for the derived value of the BH mass:

$$R_g = 2GM(\text{BH})/c^2 \approx 6.2 \times 10^{14} \text{ cm.}$$

According to our model calculations (Sect. 3.8), the bulk of $H\beta$ emission is produced at $r \approx 200 R_g$, which corresponds to a time lag $\tau = r/c \approx 48$ light days. This implies a shorter time lag than the one derived in this paper (Table 7). Can these values be reconciled? The reverberation method assumes that the FWHM of the lines reflects virialized motions, while we assumed that the motions are purely rotational. These two working hypotheses may explain differences in the size of the emitting region on the order of $\approx 40 - 50\%$. Then the time lag for $200 R_g$ could be about $\tau \approx 70$ lt.days. A value which is closer to the mean lags listed in Table 7: $\tau_{cen} \approx (86 \pm 24)$; and $\tau_{max} \approx (67 \pm 32)$. Worth, mentioning is the good agree-

ment (within 20 "cool dense material" reprocesses X-ray radiation into the Fe Kalpha line detected by Eracleous, et al. (1996).

4. Conclusions

The results of a 4-year (1995–1999) spectroscopic and broad-band BVRI photometric monitoring of the AGN 3C 390.3 are presented in this paper for the $H\beta$ spectral region.

Our main conclusions are:

1. The historical light curve in B shows a large increase of brightness during 1970–1971 followed by a gradual decrease until 1982. At that time, the nucleus of 3C 390.3 was in a minimum luminosity state. On the descending branch of the light curve, flares with an amplitude up to 1^m were observed.
2. The broad $H\beta$ and continuum fluxes vary by a factor of about three during the time interval 1995–1999.
3. Two large amplitude outbursts in the intensity of the $H\beta$ line and the continuum, with different duration were observed: (Fig. 4): in (Oct.1994-Jul.1997) – a brighter flare lasting ≈ 1000 days and another one in (Jul. 1997 – Jun. 1999) with that lasted ≈ 700 days. The event duration is defined as the interval between minima in the light curve.
4. From a cross-correlation analysis, a delay of ≈ 100 days in the response of the $H\beta$ emission with respect to the optical continuum changes is obtained from the observations at any given time. Yet, for observations obtained between the June 1997 until 1999 (JD2450618 – 2451527 – case C), a period in which the sampling was better, a shorter lag of 33 to 36 days appears jointly with the one of ≈ 100 days. In the light of these results, we have to admit that either, our data set is not suitable for an accurate determination of the delays due to a somewhat poor temporal sampling, or that the delay for 3C 390.3 varies with time, i.e. the correlation between the flux variations in the continuum and in $H\beta$ at different times is not the same. In the 8 year monitoring campaign of NGC 5548, Peterson et al. (1999) have determined, that the time delay had varied. They suggested that changes in the time delays may be related to luminosity variations of the central source. Yet, in other investigation of NGC 5548 (Netzer and Maoz, 1990) have shown, that continuum variations with a long time scale –long lasting flares– yield longer time lags. Both possibilities are present in our results for 3C 390.3 ie.: a) the continuum outburst of 1994–1997 with larger amplitude and duration (≈ 1000 days) yields a longer time lag (100 days); b) the continuum outburst in 1997–1999 of a smaller amplitude and duration (≈ 700 days) yields two lags: 100 and 35 days. We believe that both, the optical continuum and $H\beta$ flux variations reflect the changes in the X-ray irradiation, modulated by accretion rate changes. And

that the radius $H\beta$ emission zone, changes due surface temperature changes in the disk (Ulrich, 2000).

5. The observed flux for the blue and red wings of the profile varied quasi-simultaneously (Fig. 6) (i.e. whenever the flux in the blue wing increases, that in the red wing also increases). We have not detected a delay in the changes of the $H\beta$ blue wing (-7100 km s^{-1} to -1900 km s^{-1}) and of the red wing ($+1900 \text{ km s}^{-1}$ to $+7100 \text{ km s}^{-1}$) with respect to the core of the line (-1900 km s^{-1} to $+1900 \text{ km s}^{-1}$) or relative to each other. A similar result was obtained by Dietrich et al. (1998) from monitoring data for 3C 390.3 during 1994–1995. These results exclude the presence of considerable radial motions in the BLR in this object.
6. The blue-to-red wing flux ratio shows a monotonic increase with time for the period covered by our observations (Fig. 6d). The quasi-sinusoidal changes (period ≈ 10 years) of the blue-to-red bump flux ratio detected by Veilleux et al. (1991) are not present in our data for the 1995–1999 lapse.
7. The shape of the $H\beta$ profile has changed drastically: during 1996, the blue and red bump emission was very strong, while when the source was faintest (1997) the profiles had rather flat tops (Fig. 8). The blue wing was brighter than the red one during the observed period.
8. The changes of the radial velocity of the blue bump relative to the $H\beta$ narrow emission in 1995 until Oct. 1999 follow the same trend found by Eracleous et al. (1997). Their model for a binary BH with a very large mass value ($> 10^{11} M_\odot$) seems to fit our data as well. These authors argued that such a large value for the binary BH mass, is difficult to reconcile with other observations and theory. Therefore, they reject the hypothesis of a binary black hole for 3C 390.3. Our results provide further support to the dismissal of the binary BH hypothesis for 3C 390.3, on the basis of the masses required.
9. The difference profiles of the $H\beta$ broad emission revealed that the radial velocities of the blue and red bumps in the profiles varied, showing an increase in absolute value by about 2000 km s^{-1} during the observed period. From these results (Table 7, Fig. 11), it is inferred that an annular zone in the accretion disk with enhanced $H\beta$ emission could have moved towards smaller radii between 1995 and 1999, i.e. larger Keplerian velocities as the flux in the continuum decreased (Table 7). These results are in agreement with a model in which the surface temperature of the disk is modulated by the irradiation of a variable X-ray source (see Ulrich, 2000 and references therein). The X-ray variability on time scales of hours, days, weeks is, in turn, modulated by accretion rate changes. Thus, the peak velocity shifts as different profiles are also expected to result from the variable accretion rate near the black hole.
10. We have fitted the broad $H\beta$ line profiles in the framework of an accretion disk model. We obtained a satisfactory agreement for a disk with an inclination angle of about 25° and with the region of maximum emission located at about $200 R_g$. The radius of this zone is comparable to the one in which the Fe Kalpha line emission originates according to Eracleous et al. (1996).
11. The mass of the black hole in 3C390.3 estimated by the combined reverberation-rms method (Wandel, et al., 1999) is $M_{rev} \approx 2.1 \times 10^9 M_\odot$.

Our results do not support either the models of outflowing biconical gas streams or those of supermassive binary BHs. Instead, we conclude that our results favor the accretion disk model.

The velocities of the blue and red bumps and their difference, obtained from $H\beta$ difference profiles, show a distinct anticorrelation with continuum flux changes. Taking into consideration the time lag and the $H\beta$ flux, we find that the zone of maximal contribution to line emission, moves across the face of the disk. It is located at smaller radii when the flux in the continuum decreases (bump velocities increase), and to larger radii when the continuum flux increases (bump velocities decrease). These transient phenomena are expected to result from the variable rate of accretion close to the black hole. At low accretion rates, the flux from the central source may decrease by a large factor, and the integral flux in the line could decrease. Then, the maximum emission zone of the broad Balmer lines could shrink to such small radii, that the lines could become extremely broad and of low-contrast. Consequently, at those times, they would be undetectable. This may be the reason why the broad emission lines were not seen in the 3C 390.3 spectrum in 1980 (Heckman et al. 1981) or were very weak in 1984 (Penston & Perez 1984). At those times the central source brightness was at long lasting minima (Fig. 2).

It is interesting to note, that the model calculations of Nicastro (2000) point to a relationship between FWHM broad emission lines and accretion rate for a given BH mass — the lower the accretion rate the greater the line width. For different BH masses, there is a minimum value of the accretion rate, below which no broad lines are formed. The permitted interval of velocities ranges from $\approx 20000 \text{ km s}^{-1}$ for sub-Eddington accretion rates to $\approx 1000 \text{ km s}^{-1}$ for Eddington accretion rates (i.e. the lines with $\text{FWHM} > 20000 \text{ km s}^{-1}$ do not exist for any mass of the black hole).

Acknowledgements. The authors want to thank M. Eracleous for providing some of the data used in Fig.10. We would like to thank Didier Pelat for his help in the computation of the model profiles. We are thankful to G.M. Beskin for many useful discussions, to S.G. Sergeev for allowing us to use some of his software for spectral analysis tools, to O. Martinez for some spectral observations and to V.E.Zhdanova for help in data processing. This paper has had financial support from INTAS (grant N96-0328), RFBR (grant N97-02-17625, grant N00-02-16272a), scientific technical programme “Astronomy” (Russia), RFBR+CHINE (grant 99-02-39120) and CONACYT research grants G28586-E, 28499-E and 32106-E (México).

References

Alef, W., Gotz, M.M.A., Preuss, E., et al., 1988, A&A 192, 53

Alef, W., Wu, S.Y., Preuss, E., et al., 1996, A&A 308, 376

Alloin, D., et al., 1995, A&A 293, 293

Amirkhanian V. et al., 2000, Bull. Spec. Astrophys. Obs. 50, (in press)

Antokhin, I. I.; Bochkarev, N.G., 1983, AZh 60, 448

Babadzhanyants M.K., et al., 1973, Trudy AO LGU 29, 72

Babadzhanyants M.K., et al., 1974, Trudy AO LGU 30, 69

Babadzhanyants M.K., et al., 1975, Trudy AO LGU 31, 100

Babadzhanyants M.K., et al., 1976, Trudy AO LGU 32, 52

Babadzhanyants M.K., et al., 1984, Trudy AO LGU 39, 43

Barr, P., et al., 1980, MNRAS 193, 562

Barr, P., Willis, A.J., Wilson, R., 1983, MNRAS 202, 453

Baum, S.A., Heckman, T., Bridle, A., et al., 1988, ApJS 68, 643

Blanforf, R.D., McKee, C.F., 1982, ApJ 255, 419

Bochkarev, N. G., Antokhin, I., 1982, Astron. Tsirk. 1238

Bochkarev, N.G., Burenkov, A.N., and Shapovalova, A.I., 1997, Astron. & Astroph. Trans. 14, 97

Bochkarev N.G., Shapovalova A.I., Burenkov A.N., et al., 1997, Ap&SS 252, 167

Bochkarev N.G., Shapovalova A.I., 1999, PASPC 175, 75

Cannon R.D., Penston M.V., and Brett R.A., 1971, MNRAS 152, 79

Chakrabarti, S.K., and Wiita, P., 1994, ApJ 434, 518

Chen, K., Halpern, J.P., Filippenko, A.V., 1989, ApJ 339, 742

Chiang, J., Reynolds, C.S., Blaes, O.M., et al. 2000, ApJ 528, 292

Clavel, J.C., Wamsteker, W., 1987, ApJ 320, L9

Clavel, J., et al., 1991, ApJ 366, 64

Collier, S., et al., 1998, ApJ 500, 162

Collin, S., Huré J.M., 1999, A&A 341, 385

Collin, S., Huré, J.M., 2001

Cousins, A.W.J., 1976, Mem.R.Astron.Soc. 81, 25

Crenshaw, D.M., et al., 1996, ApJ 470, 322

Dietrich, M., et al., 1993, ApJ 408, 416

Dietrich, M., et al., 1998, ApJS 115, 185

Doroshenko, V.T., et al., 2001, Pis'ma v Astron. Zh. (in press)

Dumont, A.-M. Collin-Souffrin, S., 1990a, A&AS 83, 71

Dumont, A.-M., Collin-Souffrin, S. 1990b, A&A 229, 313

Dumont, A.-M., Collin-Souffrin S., Nazarova L., 1998, A&A 331, 11

Edelson, R.A., et al., 1996, ApJ 470, 364

Eracleous, M., Livio, M., Halpern, J.P., et al., 1995, ApJ 438, 610

Eracleous, M., Halpern, J.P., Livio, M., 1996, ApJ 459, 89

Eracleous, M., et al., 1997, ApJ 490, 216

Galeev, A.A., Rosner, R., Vaiana, G.S., 1979, ApJ 229, 318

Gaskell, C.M. 1983, in: Proc. 24th Liege Int. Astrophys. Colloq., Quasars and Gravitational Lenses (Cointe-Ougree:Univ. Liege), 471

Gaskell, C.M., Sparke, L.S., 1986, ApJ 333, 646

Gaskell, C.M., Peterson, B.M., 1987, ApJS 65, 1

Gaskell, C.M., 1996, ApJ, 464 L107

Gerbal, D., Pelat, D., 1981, A&A 95, 18

Heckman T.M., Miley, G.K., van Breugel, W.J.M., et al., 1981, ApJ 247, 403

Hubeny, I., Agol, E., Blaes, O., et al., 2000, ApJ 533, 710

Inda, M., et al., 1994, ApJ 420, 143

James, 1994, MINUIT : function minimization and error analysis (CERN program libr. long writeup D506)(Version 94.1; Geneva : CERN)

Johnson H.L., 1966, ARA&A 4, 193

Kaspi, S., et al., 1996, ApJ 470, 336

Korista, K.T., et al., 1995, ApJS 75, 719

Laor, A., Netzer, H., 1989, MNRAS 238, 897

Lawrence, C., et al., 1996, ApJS 107, 541

Leahy, J.P., Perley, R.A., 1991, AJ 102, 537

Leahy, J.P., Perley, R.A., 1995, MNRAS 277, 1097

Leighly, K.M., et al., 1996, ApJ 463, 158

Leighly, K.M., et al., 1997, ApJ 483, 767

Leighly, K.M. & O'Brien, P.T., 1997, ApJ 481, L15

Livio, M., Xu, C., 1997, ApJ 478, L63

Lyuty V.M., Oknyansky V.L., and Chuvaev K.K., 1984, Pis'ma v Astron. Zh. 10, 803

Maoz, D., et al., 1993, ApJ 404, 576

Neizvestny, S.I., 1986, Bull. Spec. Astrophys. Obs. 51, 5

Netzer, H., 1982, MNRAS 198, 589

Netzer, H., Maoz, D., 1990, ApJ 365, L5

Nicastro, F., 2000, ApJ 530, L65

O'Brien, P.T., et al., 1998, ApJ 509, 163

Orr, M.J.L., Browne, I.W.A., 1982, MNRAS 200, 1067

Osterbrock, D.E., Koski, A.T., Phillips, M.M., 1975, ApJ 197, L41

Penston, M.J., Penston, M.V., Sandage, A., 1971, PASP 83, 783

Penston, M.V., Perez, E., 1984, MNRAS 211, 13P

Perez, E., et al., 1988, MNRAS 230, 353

Peterson, B.M., Collins II, G.W., 1983, ApJ 270, 71

Peterson, B.M., et al., 1991, ApJ 368, 119

Peterson, B.M., 1993, PASP 105, 247

Peterson, B.M., et al., 1993, ApJ 402, 469

Peterson, B.M., et al., 1994, ApJ 425, 622

Peterson, B.M., et al., 1995, PASP 107, 579

Peterson, B.M., et al., 1998, ApJ 501, 82

Peterson, B.M., et al., 1999, ApJ 510, 659

Pica A.J., et al., 1980, AJ 85, 1442

Reichert, G.A., et al., 1994, ApJ 425, 582

Robinson, A., Perez, E., 1990, MNRAS 244, 138

Rokaki, E., Boisson, C., Collin-Souffrin, S., 1992, A&A 253, 57

Rodriguez-Pascual, P.M., et al., 1997, ApJS 110, 9

Sandage A., 1973, ApJ 180, 687

Santos-Lleo, M., et al., 1997, ApJS 112, 271

Scott R.L., et al., 1976, AJ 81, 1440

Selmes, R.A., Tritton, K.P., Wordsworth R.W. 1975, MNRAS 170, 15

Shakura, N. I., Sunyaev, R.A., 1973, A&A 24, 337

Shapovalova, A.I., Burenkov, A.N. and Bochkarev, N.G., 1996, Bull. Spec. Astrophys. Obs. 41, 28

Stirpe, G.M., et al., 1994, ApJ 425, 609

Ulrich, M.H., 2000, ESO Prepr., N1359, 1

Veilleux, S., Zheng, W., 1991, ApJ 377, 89

Vlasyuk V.V., 1993, Bull. Spec. Astrophys. Obs. 36, 107

Wamsteker, W., 1981, A&A 97, 329

Wamsteker, W., et al., 1997, MNRAS 288, 225

Wandel, A., Peterson, B.M., Malkan, M.A., 1999 ApJ 526, 579

Wanders, I., et al., 1997, ApJS 113, 69

Warwick, R., et al., 1996, ApJ 470, 349

White, R.J., Peterson, B.M., 1994, PASP 106, 879

Wozniak, P.R., et al., 1998, MNRAS 299, 449

Yee, H.K., Oke, J.B., 1981, ApJ 248, 472

Zheng, W., Veilleux, S., Grandi, S.A., 1991, ApJ 381, 121

Zheng, W., et al., 1995, AJ 109, 2355

Zheng, W., 1996, AJ 111, 1498